RSC Advances

PAPER

View Article Online
View Journal | View Issue

Cite this: *RSC Adv.*, 2021, **11**, 24613

Organic–inorganic hybrid sol–gel materials doped with a fluorescent triarylimidazole derivative†

Rui P. C. L. Sousa, [a] Rita B. Figueira, [a]‡* Bárbara R. Gomes,[a] Susana P. G. Costa, [a] Miguel Azenha,[b] Rui F. P. Pereira [a] and M. Manuela Raposo [a]

The development of sensors for pH monitoring is of extreme importance in the monitoring of concrete and reinforced concrete structures. Imidazole derivatives are promising probes for pH sensing due to the amphoteric nature of their heterocyclic ring, which can be protonated/deprotonated upon pH changes. In this work, a triarylimidazole was synthesised and used as a dopant in an organic–inorganic hybrid (OIH) sol–gel matrix to obtain a pH-sensitive membrane for further application in optical fibre sensors (OFS). The triarylimidazole probe shows fluorimetric response in pH between 9 and 13, which is the desired range for monitoring carbonation of concrete. This degradation process lowers the highly alkaline pH of concrete (12.5–13) to values below 9, which creates favourable conditions for corrosion of concrete reinforcement. The OIH membranes used were based on Jeffamine THF170 and 3-glycidoxypropytrimethoxysilane precursors, which had already been shown to be suitable and resistant in contact with cement-based materials. The OIHs were doped with three different contents of the triarylimidazole and the structural, dielectric, thermal and optical properties of the pure and doped OIH materials were evaluated. The structural analysis showed that the presence of the triarylimidazole did not change the structural properties of the OIH material. Electrochemical impedance spectroscopy showed that in the doped samples the conductivity increased with the imidazole concentration. The ε_r obtained for the doped samples ranged approximately from 11 to 19 and for the pure matrices was 8. Thermal analysis showed that these materials are stable up to 350 °C and that the presence of the probe did not change that feature. The optical properties showed that the prepared OIH materials have promising properties to be used as pH sensitive fluorimetric probes.

Received 22nd May 2021
Accepted 2nd July 2021

DOI: 10.1039/d1ra03997k

rsc.li/rsc-advances

Introduction

Concrete is generally accepted by society as a very stable material, with high durability, long service life and low maintenance costs. However, its degradation may occur due to physical or chemical factors. This may be due to carbonation of concrete, corrosion of reinforcement or alkali-silica reaction.[1,2]

Concrete structures are porous and entry of aggressive species, such as chloride ions or atmospheric CO_2, may occur. The latter can lead to carbonation of concrete, a process that is generically the chemical reaction of atmospheric CO_2 with alkaline constituents present in the concrete pore solution to form calcite ($CaCO_3$). The interstitial concrete pore solution is usually highly alkaline (pH 12.5–13). However, due to carbonation, the pH can drop to values between 6 and 9,[3] which compromises the integrity of the concrete[4] by partially creating the necessary electrochemical conditions for corrosion of the reinforcement. Therefore, monitoring the pH of concrete is essential to ensure the durability for which civil engineering structures are dimensioned and to avoid premature deterioration of the structure. The use of sensors to monitor concrete degradation is widely accepted by the civil engineering community as it provides a rational approach to evaluating repair options and planning inspection and maintenance programmes.[5] Optical fibre sensors (OFS) are considered as an interesting alternative due to their interesting advantages, *i.e.* reduced cost, size and weight, higher sensitivity and immunity to external factors.[2] The proof of this is that several OFS have been reported in recent years for application in concrete structures.[2,6–11] For instance, an OFS for chloride detection in concrete was reported by Ding and coworkers.[11] Lucigenin was immobilised on a sol–gel membrane and the presence of chloride ions quenched the fluorescence of the compound with a limit of detection of 0.02 M. OFS for pH monitoring in concrete has also been reported.[9] Tariq *et al.* reported an OFS

[a]*Centre of Chemistry, University of Minho, Campus of Gualtar, 4710-057 Braga, Portugal. E-mail: rita@figueira.pt*

[b]*ISISE, Engineering School, University of Minho, Campus of Azurém, 4800-058 Guimarães, Portugal*

† This paper is dedicated to the memory of Professor Carlos J. R. Silva who suddenly passed away on August 27th, 2020.

‡ Presently at Vasco da Gama CoLAB, Rua Roberto Frias, 4200-465 Porto, Portugal.

based on a fluorescent molecular probe enclosed in a cross-linked matrix of polyvinyl alcohol (PVA), with a response time of 100 s and a detection limit of 0.1 pH units.[10] Nevertheless, these OFS systems need to be further developed, as they have not achieved, *hitherto*, the reliability and accuracy of the destructive methods currently used.[6] One of the main advantages of OFS is that they can be easily functionalised with a sensing membrane composed of a polymer or gel with properties to detect a specific analyte.[9,11–13] In this context, the sol–gel technique is a versatile and widely used method that allows obtaining xerogels with interesting optical and dielectric properties suitable for the functionalisation of OFS.

In recent years, several OFS functionalised with sol–gel membranes have been reported, including for pH sensing.[12–18] Pathak and Singh developed a down-tapered OFS for pH monitoring using three pH indicators in a sol–gel membrane with a maximum sensitivity of 0.49 dBm pH^{-1}.[14] Timbó *et al.* also used a pH indicator (bromocresol purple) on a sol–gel matrix, resulting in a sensor with acceptable linearity between a pH of 4 and 10.[15] Bhardwaj *et al.* reported a no-core OFS using a sol–gel technique and three pH indicators to achieve a wide pH range, *i.e.*, between 2 and 13.[18] The developed sensor showed a sensitivity of 1.02 and 0.93 nm pH^{-1} for acidic and alkaline solutions, respectively. However, the application of this type of sensor in the field of civil engineering is still far from being ready for the market. Nguyen *et al.* reported the fabrication of an OFS for the pH range between 10 and 13, based on a coumarin imidazole dye covalently bonded to a polymer network.[19] The sensor showed good stability, with no photobleaching and no sensitivity to ionic strength. The authors reported that the performance of the sensor was still accurate after 20 months.

The physical and chemical properties of sol–gel materials can be tuned for the desired application by changing the precursors or synthesis conditions allowing to obtain organic–inorganic hybrid (OIH) materials.[20,21] These types of materials combine the rigidity of silicates with the flexibility and hydrophobicity of organic moieties.[22–29] The organic moieties of these materials include the commercial polyetheramines, particularly Jeffamines®, which have been frequently reported in the preparation of OIH materials.[23,25,26,30–36] The use of Jeffamines® precursors to prepare sol–gel materials can result in urea silicates or aminoalcohol silicates matrices, depending on the silane used and type of bond established *i.e.*, urea or aminoalcohol, respectively. These materials can be doped with chromo-fluorogenic chemosensors and become sensitive membranes that can be applied to OFS.

The development of chromo-fluorogenic molecular chemosensors for ions and neutral molecules has been extensively studied due to their potential applications in several scientific fields such as life sciences, medicine, chemistry, environment, *etc.*[37,38] Therefore, the development of optical pH probes, besides its application in the field of civil engineering, has attracted much attention due to the crucial role of pH in various physiological processes.[39,40] In this sense, imidazole derivatives are versatile compounds and interesting candidates as pH-sensitive molecules due to the amphoteric nature of the imidazole heterocycle. In fact, the imidazole ring can act as an excellent bond donor moiety in anion receptors since the acidity of the NH proton of the imidazole can be tuned by changing the electronic properties of the imidazole substituents. Moreover, the presence of a pyridine-like donor nitrogen atom within the ring, which is capable of selectively binding cationic species, also converts imidazoles into excellent cationic optical chemosensors.[41–43] Therefore, imidazoles can be protonated or deprotonated depending on the pH of the environment.[44,45]

Recently, triaryl (heteroaryl)-imidazole based chromophores have attracted increasing attention due to their unique optical properties (linear and nonlinear) and excellent thermal stability in guest–host systems. Thus, these heterocyclic π-conjugated systems have found application as nonlinear optical materials,[46,47] thermally stable fluorophores for OLEDs,[48] two-photon absorbing molecules,[49] DNA intercalators[50] and PDI photosensitizers.[51] In addition, they are also used as optical chemosensors in organic solvents and aqueous solutions, and as bioimaging probes for the detection of anions, neutral molecules and metal ions with biological/medical relevance.[49,52–61] Several imidazole derivatives have been used as pH sensors. Ge *et al.* reported the synthesis of a 4-phenyl-pyrido[1,2-*a*] benzimidazole-3-carboxylic acid (PPBI-1), which exhibits a fluorescence quantum yield of 0.96 and is sensitive to pH values between 4.2 and 6.4.[62] Beneto *et al.* synthesised a phenanthro [9,10-*d*]imidazole in combination with thiophene tethered pyridine (PITP).[63] The probe can be protonated or deprotonated both at the imidazole and the piperidine ring, turning this molecule into a pH sensor in two different pH ranges. Horak *et al.* reported a benzimidazole Schiff base immobilised in PVC thin films.[64] The probes showed colour changes upon protonation and fluorimetric pH sensitivity in the range of 6–7 when immobilised on the PVC matrix. Pfeifer *et al.* prepared a polyurethane hydrogel with a pH-sensitive dye perylene bisimide functionalised with one or two imidazole moieties.[65] The protonation/deprotonation of the imidazole ring allows pH sensing at alkaline pH values. The abovementioned work by Nguyen *et al.* reported an imidazole-based OFS that is sensitive to pH in the desired range for concrete applications, *i.e.*, pH 10–13.[19] This work was the first to apply the pH-sensitivity of the imidazole ring to an OFS. The authors claimed that tests of the device embedded in concrete were underway. However, as far as the authors are aware, no further progress has been reported yet.

Following our previous work on imidazole derivatives for various optoelectronic and biological applications,[46–61] along with OIH materials for concrete sensing,[66,67] the current work reports the synthesis of an imidazole derivative and the characterization of OIH materials, pure and doped with the fluorescent triarylimidazole, to evaluate the prospect of preparing pH-sensitive membranes for use in OFS to evaluate the carbonation of concrete. The synthesised OIHs were based on Jeffamine® THF170 and 3-glycidoxipropyl-trimethoxysilane, which showed suitable properties for the desired application in previous studies.[67] The structural properties of both pure and doped films were investigated by Fourier-transformed infrared spectroscopy. The dielectric properties of the films doped with

the fluorescent triarylimidazole were characterised by electrochemical impedance spectroscopy. The thermal stability was evaluated by thermogravimetric analysis. The optical properties of the OIH films doped with fluorescent triarylimidazole were investigated by UV-Visible and fluorescence spectroscopy.

Experimental

Materials

Synthesis of imidazole **1** was monitored by thin layer chromatography (0.25 mm thick pre-coated silica plates: Merck Fertigplatten Kieselgel 60 F254). NMR spectra were obtained on a Bruker Avance III 400 at an operating frequency of 400 MHz for ^{1}H and 100.6 for ^{13}C using the solvent peak as internal reference. The solvent is indicated in parenthesis before the chemical shift values (δ relative to TMS and given in ppm). Melting point (Mp) was determined on a Gallenkamp apparatus. Infrared spectra were recorded on a BOMEM MB 104 spectrophotometer in KBr pellets. Fluorescence spectrum of imidazole **1** was collected using a FluoroMax-4 spectrofluorometer. UV-visible absorption spectra (200–700 nm) were obtained using a Shimadzu UV/2501PC spectrophotometer. Luminescence quantum yield was determined by using a 10^{-6} M solution of 9,10-diphenylanthracene in ethanol as standard ($\Phi_F = 0.95$).[68] All commercially available reagents were used as received.

Commercial reagents 3-glycidoxipropyltrimethoxysilane (GPTMS) (97%, Sigma-Aldrich, St. Louis, MO, USA), Jeffamine® THF170 (Huntsman Corporation, Pamplona, Spain), calcium hydroxide ($Ca(OH)_2$, 95%, Riedel, Bucharest, Romania), potassium hydroxide (KOH, 90%, Panreac, Darmstadt, Germany), and solvents tetrahydrofuran (99.5% stabilised with ~300 ppm of BHT, Panreac, Darmstadt, Germany) and absolute ethanol (EtOH, Panreac, Darmstadt, Germany) were used as received. Commercial buffer solutions of pH 4, 7 and 9 (Panreac, Darmstadt, Germany) were used in the preliminary tests. High purity deionised water with high resistivity (higher than 18 MΩ cm) obtained from a Millipore water purification system (Milli-Q®, Merck KGaA, Darmstadt, Germany) was used.

Synthesis of imidazole derivative 1 and organic–inorganic hybrid (OIH) films

Synthesis and characterization of imidazole derivative 1. Benzaldehyde (1 mmol), diphenylethanedione (1 mmol) and NH_4OAc (20 mmol) were dissolved in glacial acetic acid (5 mL), followed by stirring and heating at reflux for 8 h. The mixture was then cooled to room temperature, ethyl acetate was added (15 mL) and washed with water (3 × 10 mL). After drying with anhydrous $MgSO_4$, the solution was filtered, and the solvent was evaporated to dryness. The resulting solid was dissolved in the minimum volume of acetone and precipitation by addition of petroleum ether afforded the pure 2,4,5-triphenylimidazole **1**,[69] as a white solid (109 mg, 65%). Mp: 272.0–272.7 °C. UV (ACN): λ_{max} nm (log ε/M^{-1} cm^{-1}) 307 (4.59). IR (KBr): ν = 3037, 2967, 2852, 2783, 2729, 2641, 1950, 1883, 1688, 1600, 1502, 1487, 1460, 1410, 1322, 1202, 1127, 1071, 967, 766, 696 cm^{-1}. ^{1}H NMR (DMSO-d_6): δ = 7.21–7.56 (m, 13H, phenyl), 8.07 (dd, J = 8.4 and 1.2 Hz, 2H, phenyl), 12.67 (s, 1H, NH) ppm. ^{13}C NMR (DMSO-d_6): δ = 125.17, 126.49, 127.04, 127.76, 128.16, 128.22, 128.44, 128.64, 128.66, 130.33, 131.06, 135.15, 137.09, 145.47 ppm.

Synthesis of the OIH films. The synthesis of OIH started with the reaction between the polyetheramine Jeffamine® THF170 and GPTMS. To a glass container with the Jeffamine® dissolved in tetrahydrofuran (THF), GPTMS was added (in a molar ratio of Jeffamine® 1 : 2 GPTMS) and the solution was stirred for 20 min 107 μL of water were added and after 10 min, imidazole derivative **1** (dissolved in ethanol, 1 × 10^{-4} M) was added (for doped films). Three different volumes (500, 900 and 1000 μL) of the imidazole derivative **1** ethanolic solution were tested. When a homogeneous mixture was obtained, the gels were casted into Teflon moulds and covered with Parafilm. The films were placed in an oven (UNB 200, Memmert, Buechenbach, Germany) and kept at 40 °C for 15 days to ensure the curing of the film and remaining solvents evaporation. For details in the synthesis steps *see* Section 3.2 and Fig. 4.

Characterization of organic–inorganic hybrid (OIH) films

Fourier-transformed infrared spectroscopy (FTIR). FTIR spectra for the four films and Jeffamine THF170 were recorded in transmittance mode on a Bomem MB104 spectrometer, by averaging 20 scans at a maximum resolution of 4 cm^{-1}. Spectra were obtained in 4000–700 cm^{-1} range on KBr pellets. KBr pellets were prepared with 1 mg of OIH films and 200 mg of KBr.

Optical analysis. UV-Visible spectra for doped OIH films were recorded in absorbance mode on a Shimadzu UV-2501 PC spectrophotometer. Spectra were obtained in the range of 250–700 nm for solid samples. Fluorescence spectra for both pure and doped OIH films were recorded on a Fluoromax – 4 Spectrofluorometer of Horiba Jovin Yvon. Spectra were obtained in the range of 300–700 nm, with different excitation wavelengths and acquired at front-face geometry at room temperature.

Electrochemical impedance spectroscopy (EIS). EIS measurements were carried out at room temperature in a Faraday cage, using a potentiostat/galvanostat/ZRA (Reference 600+, Gamry Instruments, Warminster, PA, USA). EIS measurements were used to characterize resistance, electrical conductivity, and electric permittivity of OIH disc materials, as well as their capacitance. The disc films were placed between two parallel Au electrodes (10 mm diameter and 250 μm thickness) using a support cell as reported in previous studies[23] and, the EIS measurements were performed. The EIS measurements were accomplished by applying a 10 mV (peak-to-peak, sinusoidal) electrical potential within a frequency range from 1 × 10^{6} Hz to 0.01 Hz (10 points per decade) at open circuit potential. The frequency response data of the studied electrochemical cells were displayed in a Nyquist plot, using a Gamry ESA410 Data Acquisition software that was also used for data fitting purposes.

Thermogravimetric analysis (TGA). TGA was carried out on an SDT Q600 system for the OIH materials. Samples were subjected to a temperature ramp of 15 °C min^{-1} between room temperature and 750 °C at a constant 100 mL min^{-1} nitrogen

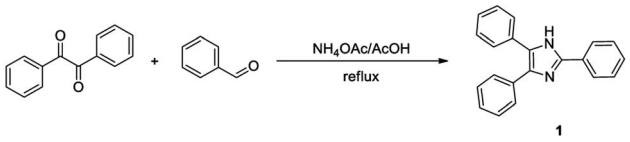

Scheme 1 Synthesis of imidazole derivative **1**.

flux. For each analysis, 20–30 mg of each OIH material was placed into an alumina pan.

Results and discussion

Synthesis and characterization of imidazole derivative 1

Imidazole derivative **1** was synthesised in 65% yield through the Radziszewski reaction of diphenylethanedione with benzaldehyde and ammonium acetate in refluxing glacial acetic acid for 8 h (*vide* Scheme 1). Earlier, the synthesis of compound **1** (2,4,5-triphenylimidazole, trivially known as lophine) was reported in a lower yield (42%) using a similar synthetic procedure.[69] Compound **1** was characterised by NMR, IR and UV-Visible (absorption and emission) spectroscopies. The absorption (λ_{max} = 307 nm) and emission spectra (λ_{max} = 384 nm) of imidazole **1** were measured in acetonitrile (ACN) solutions. The relative fluorescence quantum yield was determined by using a 10^{-6} M solution of DPA in ethanol as standard ($\Phi_F = 0.95$).[68] Imidazole **1** exhibited a good fluorescence quantum yield (0.64) in ACN.

The imidazole derivative **1**, hereafter mentioned as triarylimidazole, was tested using four solutions with different pH values to assess its optical properties change resulting from the protonation/deprotonation of the imidazole heterocycle (*vide* Fig. 1).

A simulative concrete pore solution (SCPS) with a pH of 12.5 was prepared by addition of 0.2 M KOH to a $Ca(OH)_2$ saturated solution.[70,71] Three commercial buffer solution of pH 4, 7 and 9 were used for comparison purposes (*vide* Fig. 1 and 2).

Fig. 2 and 3 show clearly the difference between the fluorescence emission obtained for a pH = 9 and a pH = 12.5, which is the working range of interest in concrete. It can be observed

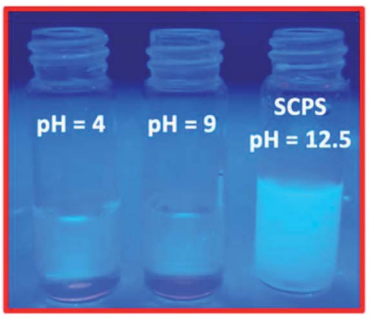

Fig. 2 Photoluminescence of triarylimidazole on a viewing cabinet under UV lamp at 365 nm at different pH solutions, *i.e.*, 4, 9 and, 12.5.

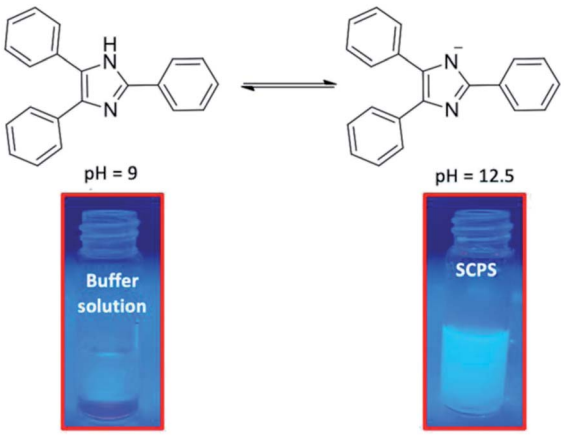

Fig. 3 Optical response of triarylimidazole in commercial buffer solution of pH 9 and in SCPS (pH = 12.5) on a viewing cabinet under UV lamp at 365 nm. The loss of the proton in alkaline media is also schematised.

that fluorescence emission increases at high pH values, *i.e.*, at pH ~12.5 (*vide* Fig. 1 and 2).

Synthesis of organic–inorganic hybrid (OIH) films. OIH materials based on the polyetheramine Jeffamine THF170 were synthesised to test the possibility of preparing highly sensitive pH-sensing membranes to be applied on OFS. Jeffamine

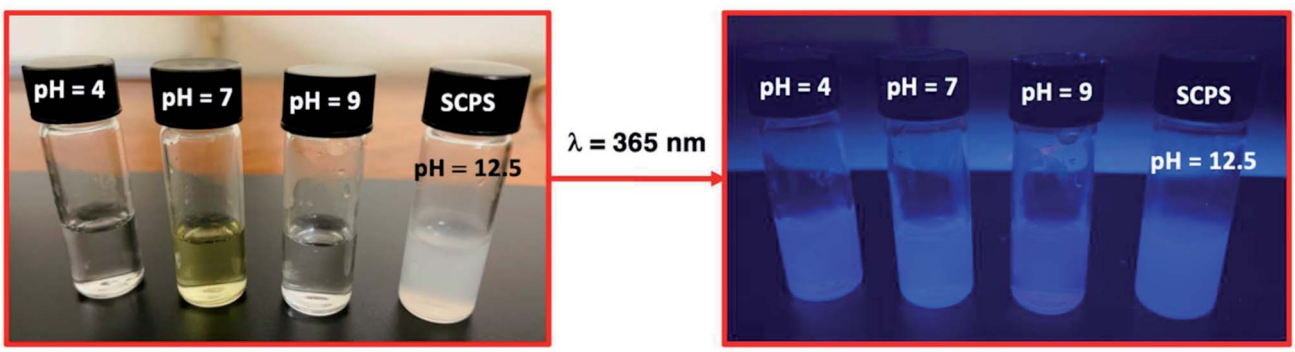

Fig. 1 Photoluminescence behaviour of triarylimidazole in different pH solutions, *i.e.*, 4, 7, 9 and, 12.5, before and after an excitation with a light with a wavelength of 365 nm.

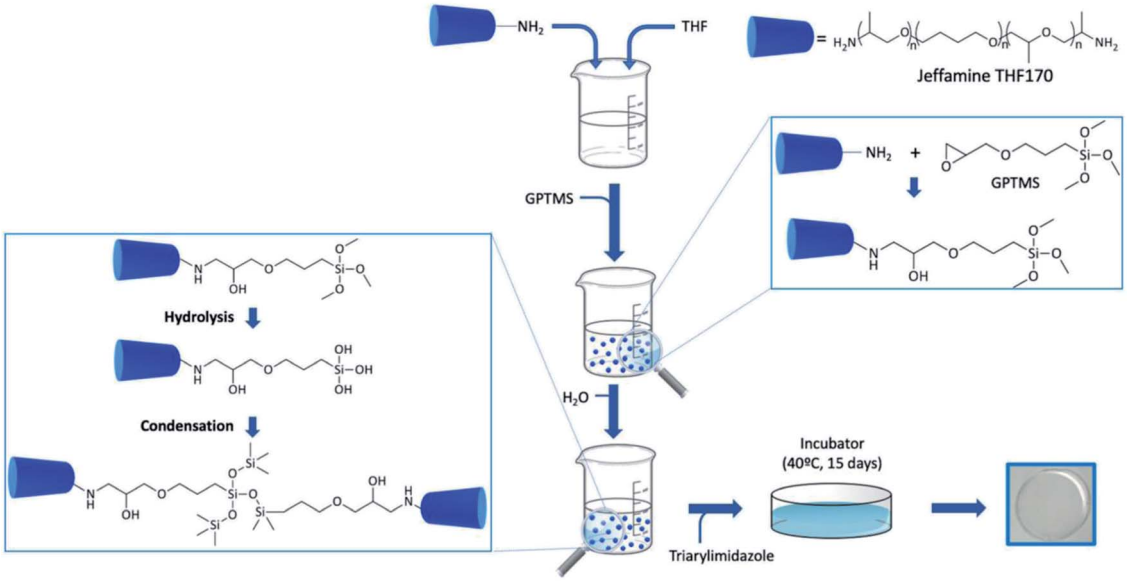

Fig. 4 Synthesis of the OIH sol–gel matrices.

THF170 reacted with GPTMS to yield the aminoalcohol precursor of the sol–gel reaction according to the procedure reported previously.[67] The precursor was subjected to hydrolysis and condensation, and the sols were then doped with the pH-sensitive fluorescent imidazole derivative 1. OIHs materials with three different contents were prepared, namely by adding 500, 900 and 1000 μL of ethanolic triarylimidazole solution (1×10^{-4} M). The main synthesis steps are schematically shown in Fig. 4. The films were designated as A(170)@500, A(170)@900 and A(170)@1000, where the numbers 500, 900 and 1000 represent the volume of imidazole solution added. The dielectric, thermal and optical properties of the pure and doped materials were evaluated.

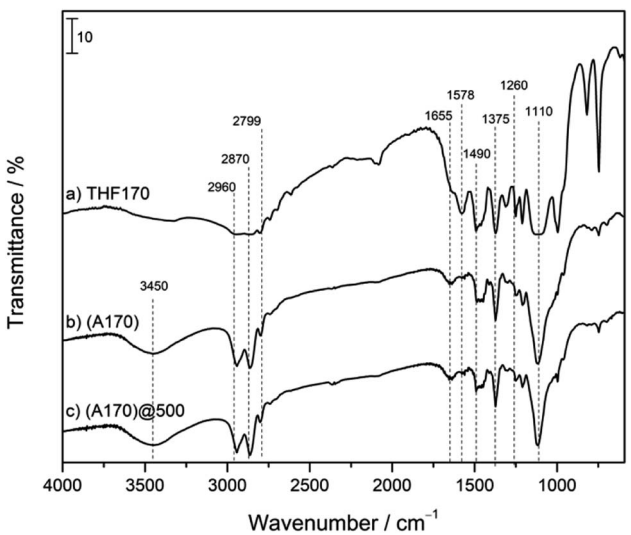

Fig. 5 FTIR transmittance spectra of: (a) Jeffamine THF170; (b) pure A(170) OIH; (c) A(170)@500.

Fourier-transformed infrared spectroscopy (FTIR). FTIR analysis was performed for the films obtained as well as for the A(170) pure matrix and the precursor Jeffamine THF170. The spectra of the precursor and the pure and doped OIH materials are shown in Fig. 5.

The spectrum of Jeffamine THF170 (a) shows bands at 2960, 2870 and 2799 cm^{-1}, characteristic of C–H stretching vibrations.[72] The band at 1578 cm^{-1} can be assigned to the bending of the terminal NH group in the Jeffamine chain. The bands at 1490 and 1375 cm^{-1} are assigned to simple bending vibrations of the carbon backbone of the polyetheramine.[72]

The GPTMS infrared spectrum has been reported previously[73] and shows a small peak at 3050 cm^{-1} assigned to the epoxide ring. A sharp peak at 2840 cm^{-1} as well as the peak at 1190 cm^{-1} and the broad band between 1100–1080 cm^{-1} are assigned to the Si-alkoxy group. These three signals are characteristic of Si–OCH_3 groups. The peak between 780–760 cm^{-1} is due to the Si–CH_3, which are typical of trialkoxysilanes. The spectrum of the pure OIH material (Fig. 5b) has a broad band at 3400–3500 cm^{-1} that can be attributed to the O–H groups in the polyether chain which resulted from the aminoalcohol bond formation.[73] O–H bonds from water molecules that may still be trapped in the polymeric hybrid may also affect this band. The bands at 2960 and 2870 cm^{-1} are caused by the asymmetric and symmetric C–CH_2 stretching vibrations, respectively. The bands at 1490 and 1375 cm^{-1}, also seen in the Jeffamine spectrum, are also present and confirm that the structural backbone of this precursor had not changed.[72] The bond formed between the two precursors is an aminoalcohol bond, the presence of which can also be confirmed by the small peak at 1655 cm^{-1}, typical of the C–NH–C bond bending vibration. The disappearance of the epoxy signal (3050 cm^{-1}) from GPTMS also confirms that the reaction between the two precursors was successful. Moreover, the other characteristic signals of this precursor (peak at

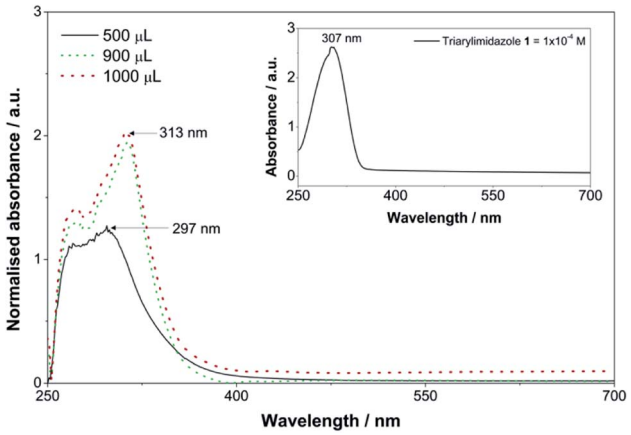

Fig. 6 UV-Visible absorption spectra of the OIH films as inset spectra of triarylimidazole.

1190 cm^{-1}, broad band between 1100–1080 cm^{-1} and broad band between 780–760 cm^{-1}) also disappeared, showing that the hydrolysis of the silane has taken place.[73,74] The small peak at 1260 cm^{-1} can be assigned to the symmetric C–Si bond bending.[74] The peak at 1110 cm^{-1} is related to Si–O–Si bonds, which are characteristic of this crosslinked OIH material.[74] It can be observed that there are no significant changes between the pure (b) and doped (c) spectra, implying that the presence of the triarylimidazole in the matrix does not change the structural properties of the material. The spectra obtained for A(170)@900 and A(170)@1000 show the same typical bands as A(170)@500 and are therefore not shown in Fig. 5.

Optical analysis. In a previous study, it was reported that A(170) matrices have promising properties to be doped with chemosensors.[67] In this study, this type of matrix was doped with triarylimidazole, which has an absorption λ_{max} of 307 nm. Fig. 6 shows the optical absorbance spectra as a function of wavelength obtained for the synthesised xerogel films doped with triarylimidazole. A baseline was plotted using a pure A(170) film and the data were normalised to the film thickness of each sample. Inset, the spectrum of triarylimidazole is also shown in Fig. 6.

Fig. 6 shows that the triarylimidazole was successfully doped into the prepared OIH films, as the peak of this compound is present. Moreover, the intensity of the band increases with increasing concentration of triarylimidazole. It can also be observed that a small bathochromic shift of 6 nm in the absorption maxima occurred in the OIH films doped with 900 μL and 1000 μL. However, Fig. 6 also shows that the samples doped with 500 μL do not match those doped with higher amounts of triarylimidazole. Moreover, the peaks show low intensity and resolution and a hypsochromic shift of 10 nm. The low content of triarylimidazole within the OIH matrix could be the reason for this behaviour. Nevertheless, no further conclusions can be drawn from these results.

To complement the optical characterization of these materials, the OIH matrices based on A(170) were also analysed by fluorescence spectroscopy. Previous studies showed that the OIH materials exhibit intrinsic emission due to photoinduced proton transfer between NH_3^+/NH^- defects and electron–hole recombination occurring in the siloxane nanoclusters.[67,75] Studies on pure A(170) OIH matrices showed that the wavelength of the emission peak shifts to longer wavelengths as the excitation wavelength increases.[67] It was shown that this dependence on excitation energy is related to transitions between localised states in non-crystalline structures and that the maximum emission wavelength is defined by the hierarchy of the silica backbone.[75,76] The four OIH materials were analysed

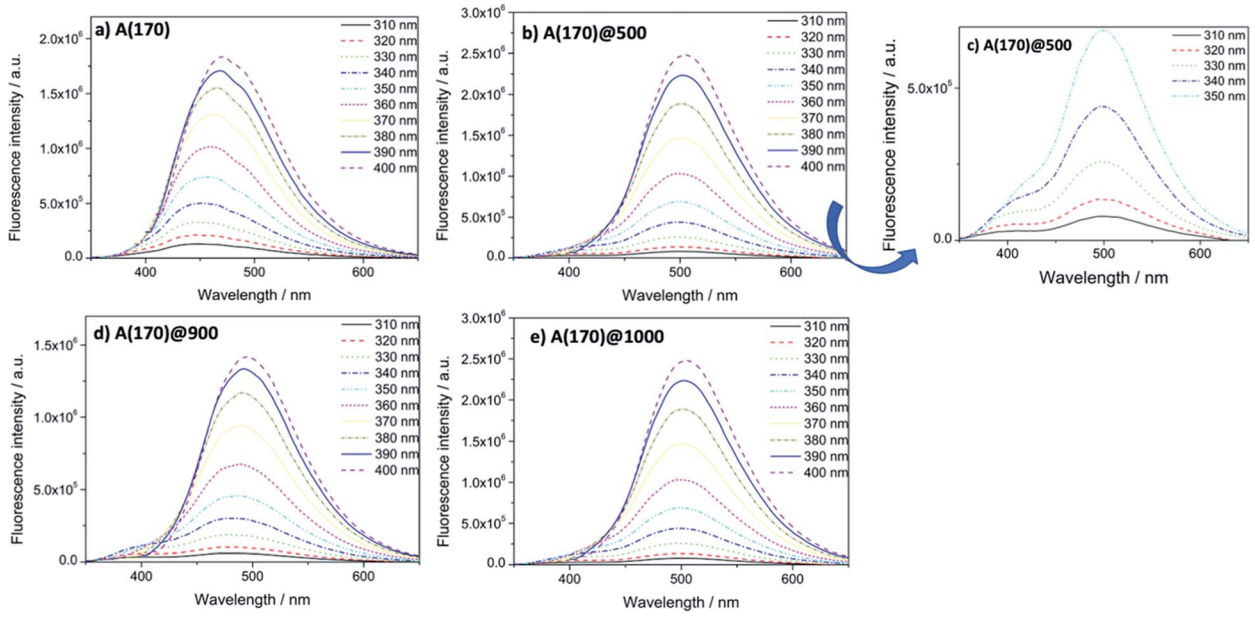

Fig. 7 Fluorescence emission spectra of the OIH films, with excitation energies between 310 and 400 nm. (a) A(170); (b) A(170)@500; (c) detail of A(170)@500 for lower λ_{exc} (310, 320, 330 and 340 nm); (d) A(170)@900; (e) A(170)@1000.

with different excitation wavelengths, from 310 to 400 nm. Fig. 9 shows fluorescence spectra obtained for the four matrices pure and doped with the triarylimidazole. It can be observed that the intensity and position of the photoluminescence emission strongly depends on the excitation wavelength and increases for all doped samples compared to undoped OIHs.

All photoluminescence emission spectra show broad bands at higher excitation energies. As the excitation energy decreases, the emission intensity of the bands increases, and the position of the emission peak shifts the lower energies. The same behaviour was observed for all doped samples.

All doped samples show two emission photoluminescence bands at $\lambda_{exc} = 310$, 320, 330, 340 and 350 nm (*vide* Fig. 7(b and c)), which shift to shorter wavelengths with increasing excitation wavelength. The photoluminescence emission band at lower energies arises from intrinsic matrix emission and slightly changes its position with increasing excitation wavelength. The full width at half maximum decreased in all spectra with the decrease of excitation energy.

The maximum emission wavelength of the pure matrix shows a bathochromic shift from 448 nm ($\lambda_{exc} = 310$ nm) to 471 nm ($\lambda_{exc} = 400$ nm). The presence of the triarylimidazole provokes a bathochromic shift in the matrix emission. In general, the maximum emission wavelength increases to values around 500 nm. The results of FTIR, UV-Visible and fluorescence spectroscopy are in agreement and prove that the triarylimidazole doped OIHs were successfully synthesised.

Electrochemical impedance spectroscopy (EIS). EIS is a technique widely used in material characterization to evaluate the dielectric properties of the OIH films.[77] The Nyquist plots obtained by this technique show the capacitive response over a wide frequency range and the dielectric properties of the material can be evaluated in the high-frequency range of these plots. In this work, EIS was used to characterise the dielectric properties (*e.g.*, conductivity, capacitance, and electrical permittivity) that can be used to assess the potential of OIH films to be used in concrete. It has already been shown that samples with resistances values above $10^7\ \Omega\ cm^2$ are suitable for the concrete environment.[78,79]

Fig. 8 shows the Nyquist plots of the pure A(170) films and the triarylimidazole doped films together with the fitting results

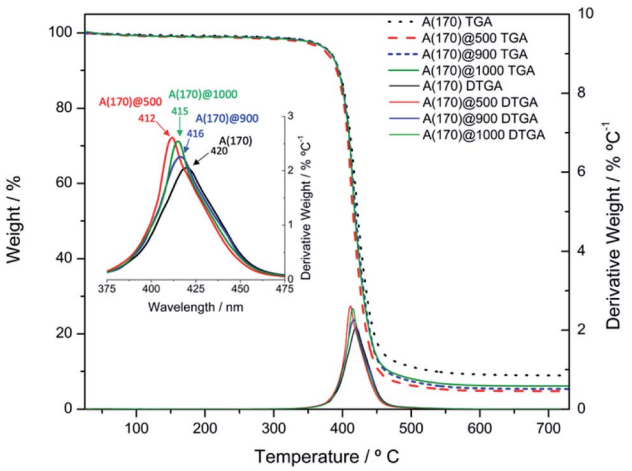

Fig. 9 TGA and DTGA traces for the OIH films.

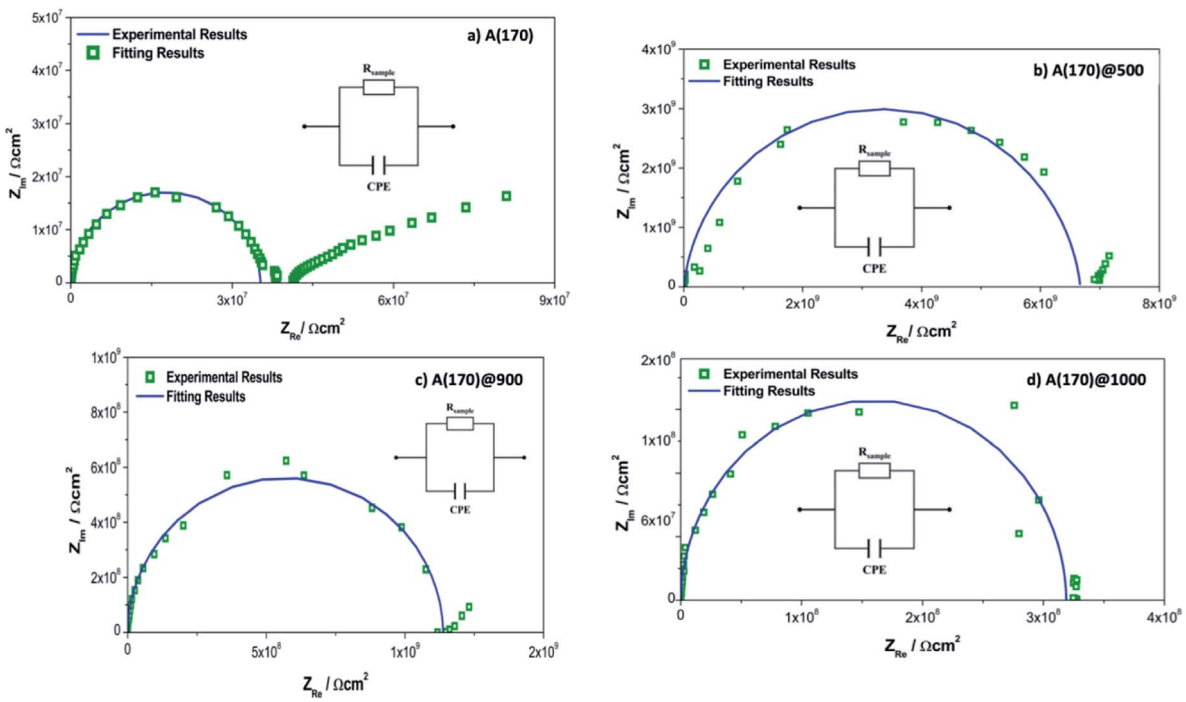

Fig. 8 Nyquist plots obtained for the OIH films: (a) pure A(170) OIH;[67] (b) A(170)@500; (c) A(170)@900; (d) A(170)@1000. All the Nyquist plots show the EEC inset.

Table 1 Results obtained for the elements of the proposed EEC obtained from EIS data fitting of the OIH materials and errors in percentage. For comparison purposes the data reported for the undoped matrix A(170)[67] was also include

OIH sample	R_{sample}/Ω	CPE $(Q)/S^{\alpha}\ \Omega^{-1}$	α	χ^2
A(170)[67]	3.53×10^7 ($\pm$0.77%)	4.76×10^{-12} ($\pm$2.29%)	0.98 (ref. 67)	3.20×10^{-4}
A(170)@500	6.67×10^9 ($\pm$1.42%)	1.40×10^{-11} ($\pm$2.07%)	0.93	2.69×10^{-2}
A(170)@900	1.14×10^9 ($\pm$1.23%)	5.43×10^{-12} ($\pm$1.25%)	0.99	8.06×10^{-4}
A(170)@1000	3.19×10^8 ($\pm$1.04%)	4.74×10^{-12} ($\pm$1.55%)	0.99	1.69×10^{-3}

and the electrical equivalent circuit (EEC) describing the impedance spectrum.

At higher frequencies, all Nyquist plots describe a semicircle intersecting the x axis. The amplitudes of the different samples change with their composition, suggesting that the concentration of triarylimidazole interferes with the impedance magnitudes by changing the dielectric properties of the OIH materials (*e.g.*, resistivity and capacitance). The data obtained at lower frequencies suggest a different electrochemical process attributed to the Au|OIH material interface, as already discussed in previous manuscripts.[66,67,78] Therefore, it will not be discussed in detail here.

The analysis of the EIS data was performed based on the EEC presented. Since the obtained results do not show ideal behaviour, constant phase elements (CPE) were used instead of pure capacitance to improve the data fitting.[66,67,78,80] The fitting parameters, including the resistance of the OIH films (R_{sample}), CPE, the percentage of associated error, α, and the goodness of the fitting (χ^2) are shown in Table 1.

According to Table 1, the resistance of the triarylimidazole doped OIHs range from 10^8 to 10^9 Ω. The resistance of the doped OIH films increases compared to the undoped ones. However, comparing different contents of triarylimidazole within the OIH matrices, the resistance decreases, *i.e.*, higher contents of triarylimidazole lead to a decrease in resistance. Nevertheless, samples doped with 1000 μL of triarylimidazole show higher resistance than pure membranes. Also, the χ^2 obtained for the data fitting is satisfactory considering that it is very low and ranges between 10^{-4} and 10^{-2}. The values obtained for the elements of the EEC in Table 1, namely R_{sample}, CPE and α, were used to obtain the effective capacitance (C_{eff}) using the relationship of Brug *et al.*[81] The values of resistance (R) and capacitance (C) were normalised to the dimensions of the cell geometry. R was determined using eqn 1 and C using eqn (2).

$$R = R_{sample} \times A_{Au\ disc} \quad (1)$$

$$C = C_{eff}/A_{Au\ disc} \quad (2)$$

The conductivity (σ) was obtained using the following relation $\sigma = (d_{sample}/A_{Au\ disc})/R_{sample}$. The relative permittivity (ε_r) was determined using the known equation $\varepsilon_r = ((C_{eff} \times d_{sample})/\varepsilon_0) \times A_{Au\ disc}$. The A_{Au} stands for the area of the gold electrodes, d_{Sample} for the thickness of the analysed OIH film sample and, ε_0 stands for the vacuum permittivity.

According to Table 2, the C values obtained for OIH doped samples are between 10^{-3} and 10^{-2}. The lowest value was given by the samples doped with 900 μL of triarylimidazole. Table 2, also shows that A(170) samples doped with triarylimidazole show higher normalised resistance (R) and dielectric constant (ε_r) values than the undoped ones. The ε_r for doped samples are between 11 and 19. It can be also observed that as the content of triarylimidazole increases, the values of R and ε_r decrease. Conductivity (σ) is mainly determined by the content of inorganic substances, hydroxyl groups and water molecules within the membrane. Table 2 shows, that for doped samples, σ values are between 10^{-11} and 10^{-10} S cm^{-1}. Doped samples show lower values compared to undoped ones.[82] However, when comparing within doped samples it can be observed that as the content of triarylimidazole increases the σ increases. This behaviour is according to the results obtained by the author Thanganathan[82] in which it was reported that the ionic conductivity increased with the imidazole concentration. These results suggest that this behaviour is related to the number of mobile charge carriers within the OIH matrix.[82]

Thermogravimetric Analysis. Fig. 9 shows that the highest degradation processes occur between 375 and 450 °C.

The obtained results are in agreement with the results found in the literature, in which it was reported that the major degradation processes in amino–alcohol based OIH materials occurred between 350–500 °C.[34,73,83,84] The degradation processes are explained by the depolymerization of the polyether material and condensation of residual Si–OH groups.[34]

Table 2 Electrical and dielectric properties of the OIH samples based on A(170) matrices doped with different contents of triarylimidazole derivative. For comparison purposes the data reported for the undoped matrix A(170)[67] was also included

OIH sample	log R/Ω cm^2	C/nF cm^2	ε_r	$-\log \sigma$/S cm^{-1}
A(170)[67]	7.03 $\pm$ 0.72	$5.01 \times 10^{-3} \pm 2.10 \times 10^{-5}$	8.12 $\pm$ 0.03	7.87 $\pm$ 0.72
A(170)@500	9.74 $\pm$ 0.03	$1.78 \times 10^{-2} \pm 1.79 \times 10^{-3}$	18.93 $\pm$ 1.36	10.91 $\pm$ 0.03
A(170)@900	8.85 $\pm$ 0.30	$7.87 \times 10^{-3} \pm 4.03 \times 10^{-3}$	15.99 $\pm$ 0.87	9.73 $\pm$ 0.30
A(170)@1000	8.37 $\pm$ 0.04	$5.73 \times 10^{-3} \pm 7.67 \times 10^{-5}$	11.37 $\pm$ 0.15	9.13 $\pm$ 0.04

Table 3 T_5, T_{max} and char yield obtained for the OIH films (data obtained from the TGA and DTGA traces)

OIH sample	T_5 (°C)	T_{max} (°C)	Char yield (%)
A(170)	380	420	8.9
A(170)@500	376	412	4.7
A(170)@900	381	416	5.3
A(170)@1000	380	415	6.1

Table 3 shows the 5% weight loss temperature (T_5), the temperature of maximum rate of weight loss (T_{max}) and char yield. No major changes on the thermal profile of the material occurred in the doped OIH films.

The T_{max} obtained for the doped samples suffered a small shift to lower temperature values. This can be linked to the lower crosslinking density,[73,83,84] which may indicate that the triarylimidazole contributes to reduce the crosslinking density of the OIH matrix. This behaviour was expected and is according to the literature.[82] This assumption can also be supported by the char yield values, that shows that the pure OIH material has a higher residual weight at 750 °C, suggesting higher crosslinking density. The char yield also increases (Table 3) with the content of triarylimidazole suggesting that the crosslinking of the doped samples decreases as the content of triarylimidazole increases. This may be correlated with the EIS data obtained for OIH doped samples since the conductivity increases as the triarylimidazole content increases. Lower crosslinking allows higher number of mobile charge carriers within the OIH matrix.[82] The results obtained (Fig. 9 and Table 3) showed that no relevant degradation processes occurred at temperatures below 350 °C. Considering all the above exposed and the fact that the normal applications of concrete are made at service temperatures within extreme ranges between −20 °C to 60 °C (as an estimate of an envelope of environmental temperatures worldwide), it can be assumed that the produced OIH films are suitable to be applied in concrete. This assumption of stability can also be taken at early stages of curing of concrete in the first few days: in fact, due to exothermic nature of cement hydration reactions, internal heat is accumulated, and temperature rises are expected, yet normally do not reach values above 70 °C,[85] which is also important to avoid other types of damage of microstructure of the hardened concrete. However, in case of fire hazard temperatures reached inside concrete can be over 1000 °C, therefore permanent and irreversible damage is expected to the films and optical fibres.

Conclusions

An imidazole derivative (triarylimidazole) was synthesised in a 65% yield. The obtained compound was characterised by NMR, FTIR and UV-Visible absorption and fluorescence spectroscopies and showed absorption λ_{max} at 307 nm and emission λ_{max} at 384 nm. The compound was tested in solutions with different pH values and showed fluorimetric changes with pH variations. Innovative OIH sol–gel materials based on Jeffamine THF170 and GPTMS doped with the triarylimidazole were reported for the first time and characterised by FTIR, UV-Visible spectroscopy, fluorescence spectroscopy, EIS and TGA.

FTIR spectroscopy showed that the synthesis of the OIHs was successful, and that the presence of the doped imidazole did not alter the structural properties of the hybrid membranes. UV-Visible and fluorescence data suggest that the samples have optical properties with potential to be used as sensing membranes for monitoring pH in alkaline environments. However, further studies need to be carried out to clarify some aspects, namely the behaviour of the membranes doped with lower levels of imidazole derivative. The dielectric properties of the materials show that within the doped samples, the conductivity increased with the imidazole derivative content. The ε_r obtained for the doped samples is approximately between 11 and 19 and, 8 for pure OIH matrix. The thermogravimetric analysis showed that the OIH films are thermally stable for application in fresh concrete since the degradation processes take place at temperature values much higher than the curing temperatures of concrete.

The obtained results suggest that the synthesised doped OIH membranes have promising properties for application in the functionalization of OFS for monitoring the pH of concrete. Nevertheless, the responsiveness of the OIH membranes deposited on OFS with pH variation needs to be evaluated and validated to reach the next stage of development.

Author contributions

Conceptualization: R. B. Figueira; formal analysis: R. B. Figueira, R. P. C. L. Sousa, B. R. Gomes, R. F. P. Pereira, M. M. M. Raposo, S. P. C. Costa; funding acquisition: R. B. Figueira and C. J. R. Silva; methodology: R. B. Figueira, R. F. P. Pereira, M. M. M. Raposo, S. P. C. Costa; investigation: R. B. Figueira, B. R. Gomes; writing – original draft preparation: R. P. C. L. Sousa, R. B. Figueira, B. R. Gomes, M. M. M. Raposo, S. P. C. Costa; writing – review and editing: R. B. Figueira, R. P. C. L. Sousa, R. F. P. Pereira, M. M. M. Raposo, S. P. C. Costa, M. Azenha; project administration: R. B. Figueira; resources: R. B. Figueira, R. F. P. Pereira, M. M. M. Raposo, S. P. C. Costa, M. Azenha; supervision: R. B. Figueira. All authors have read and agreed to the published version of the manuscript.

Conflicts of interest

There are no conflicts to declare.

Acknowledgements

Thanks are due to Fundação para a Ciência e Tecnologia (FCT) and FEDER (European Fund for Regional Development)-COMPETE-QRENEU for financial support through the Chemistry Research Centre of the University of Minho (Ref. CQ/UM (UID/QUI/00686/2019 and UID/QUI/00686/2020)), project "Sol-Sensors — Development of Advanced Fiber Optic Sensors for Monitoring the Durability of Concrete Structures"

(www.solsensors.eu), reference POCI-01-0145-FEDER-031220, and a PhD grant to Rui P. C. L. Sousa (SFRH/BD/145639/2019). The NMR spectrometer Bruker Avance III 400 is part of the National NMR Network (PTNMR) and are partially supported by Infrastructure Project No 022161 (co-financed by FEDER through COMPETE 2020, POCI and PORL and FCT through PIDDAC). Thanks are also due to FCT/MCTES through national funds (PIDDAC) under the R&D Unit Institute for Sustainability and Innovation in Structural Engineering (ISISE), under reference UIDB/04029/2020.

References

1 R. B. Figueira, R. Sousa, L. Coelho, M. Azenha, J. M. de Almeida, P. A. S. Jorge and C. J. R. Silva, *Constr. Build. Mater.*, 2019, **222**, 903–931.
2 S. Taheri, *Constr. Build. Mater.*, 2019, **204**, 492–509.
3 N. B. Winter, *Understanding cement: an introduction to cement production, cement hydration and deleterious processes in concrete*, Microanalytics Consultants, St. Ives, UK, 2012.
4 L. J. Parrott, *A review of carbonation in reinforced concrete, Cement and Concrete Association*, Wexham Springs, Liverpool, UK, 1987.
5 R. B. Figueira, *Appl. Sci.*, 2017, **7**, 1157.
6 A. Behnood, K. Van Tittelboom and N. De Belie, *Constr. Build. Mater.*, 2016, **105**, 176–188.
7 C. K. Y. Leung, K. T. Wan, D. Inaudi, X. Bao, W. Habel, Z. Zhou, J. Ou, M. Ghandehari, H. C. Wu and M. Imai, *Mater. Struct.*, 2015, **48**, 871–906.
8 A. Khadour and J. Waeytens, in *Eco-Efficient Repair and Rehabilitation of Concrete Infrastructures*, ed. F. Pacheco-Torgal, R. E. Melchers, X. Shi, N. D. Belie, K. V. Tittelboom and A. Sáez, Woodhead Publishing, 2018, pp. 97–121.
9 P. A. M. Basheer, K. Grattan, T. Sun, A. Long, D. O. Mcpolin and W. Xie, *Proc. SPIE 5586, Advanced Environmental, Chemical, and Biological Sensing Technologies II*, 7 December 2004.
10 A. Tariq, J. Baydoun, C. Remy, R. Ghasemi, J. P. Lefevre, C. Mongin, A. Dauzères and I. Leray, *Sens. Actuators, B*, 2021, **327**, 128906.
11 L. Ding, Z. Li, Q. Ding, X. Shen, Y. Yuan and J. Huang, *Sens. Actuators, B*, 2018, **260**, 763–769.
12 S. Islam, H. Bakhtiar, N. Bidin, S. Riaz and S. Naseem, *J. Sol-Gel Sci. Technol.*, 2018, **86**, 42–50.
13 S. Islam, R. A. Rahman, Z. B. Othaman, S. Riaz and S. Naseem, *J. Ind. Eng. Chem.*, 2015, **23**, 140–144.
14 A. K. Pathak and V. K. Singh, *Optik*, 2017, **149**, 288–294.
15 Á. P. Timbó, P. V. F. Pinto, H. A. Pinho, L. P. de Moura, J. B. Chretien, F. W. Viana, R. G. D. Filho, E. B. da Silva, M. E. R. da Silva, J. W. M. Menezes, G. de F. Guimarães and W. B. Fraga, *Sens. Actuators, B*, 2016, **223**, 406–410.
16 D. Razo-Medina, E. Alvarado-Méndez and M. Trejo-Durán, *Procedia Technol*, 2017, **27**, 271–273.
17 N. Deepa and A. Balaji Ganesh, *Measurement*, 2015, **59**, 337–343.
18 V. Bhardwaj, A. K. Pathak and V. K. Singh, *J. Biomed. Opt.*, 2017, **22**, 057001.
19 T. H. Nguyen, T. Venugopala, S. Chen, T. Sun, K. T. V. Grattan, S. E. Taylor, P. A. M. Basheer and A. E. Long, *Sens. Actuators, B*, 2014, **191**, 498–507.
20 H. K. Schmidt, *J. Non-Cryst. Solids*, 1985, **73**, 681–691.
21 J. D. Mackenzie, *J. Sol-Gel Sci. Technol.*, 1994, **2**, 81–86.
22 R. B. Figueira, R. Sousa and C. J. R. Silva, in *Advances in smart coatings and thin films for future industrial and biomedical engineering applications*, Elsevier, Amsterdam, Netherlands, 2020, pp. 57–97.
23 R. Figueira, E. Callone, C. Silva, E. Pereira and S. Dirè, *Materials*, 2017, **10**, 306.
24 P. Kumar, A. K. Yadav, A. G. Joshi, D. Bhattacharyya, S. N. Jha and P. C. Pandey, *Mater. Charact.*, 2018, **142**, 593–601.
25 R. B. Figueira, C. J. R. Silva and E. V. Pereira, *J. Coat. Technol. Res.*, 2014, **12**, 1–35.
26 R. B. Figueira and C. J. R. Silva, in *Hybrid Organic-Inorganic Interfaces*, Wiley-VCH Verlag GmbH & Co. KGaA, Weinheim, Germany, 2017, pp. 355–412.
27 A. C. Ianculescu, C. A. Vasilescu, M. Crisan, M. Raileanu, B. S. Vasile, M. Calugaru, D. Crisan, N. Dragan, L. Curecheriu and L. Mitoseriu, *Mater. Charact.*, 2015, **106**, 195–207.
28 N. Boaretto, A. Bittner, C. Brinkmann, B. E. Olsowski, J. Schulz, M. Seyfried, K. Vezzù, M. Popall and V. Di Noto, *Chem. Mater.*, 2014, **26**, 6339–6350.
29 A. Mujahid, P. A. Lieberzeit and F. L. Dickert, *Materials*, 2010, **3**, 2196–2217.
30 M. Špírková, P. Duchek, A. Strachota, R. Poręba, J. Kotek, J. Baldrian and M. Šlouf, *J. Coat. Technol. Res.*, 2011, **8**, 311–328.
31 M. Spírková, J. Brus, D. Hlavatá, H. Kamisová, L. Matejka and A. Strachota, *Surf. Coat. Int., Part B*, 2003, **86**, 187–193.
32 J. Brus, M. Špírková, D. Hlavatá and A. Strachota, *Macromolecules*, 2004, **37**, 1346–1357.
33 M. Špírková, J. Brus, D. Hlavatá, H. Kamišová, L. Matějka and A. Strachota, *J. App. Polym. Sci.*, 2004, **92**, 937–950.
34 R. B. Figueira, C. J. R. Silva and E. V. Pereira, *J. Coat. Technol. Res.*, 2016, **13**, 355–373.
35 V. Bekiari and P. Lianos, *J. Hazard. Mater.*, 2007, **147**, 184–187.
36 A. Sánchez-Ferrer, D. Rogez and P. Martinoty, *Macromol. Chem. Phys.*, 2010, **211**, 1712–1721.
37 P. A. Gale and C. Caltagirone, *Coord. Chem. Rev.*, 2018, **354**, 2–27.
38 D. Wu, A. C. Sedgwick, T. Gunnlaugsson, E. U. Akkaya, J. Yoon and T. D. James, *Chem. Soc. Rev.*, 2017, **46**, 7105–7123.
39 J. T. Hou, W. X. Ren, K. Li, J. Seo, A. Sharma, X. Q. Yu and J. S. Kim, *Chem. Soc. Rev.*, 2017, **46**, 2076–2090.
40 S. Halder, A. Hazra and P. Roy, *J. Lumin.*, 2018, **195**, 326–333.
41 P. Molina, A. Tárraga and F. Otón, *Org. Biomol. Chem.*, 2012, **10**, 1711–1724.
42 J. Kulhánek and F. Bureš, *Beilstein, J. Org. Chem.*, 2012, **8**, 25–49.
43 S. Kashyap, R. Singh and U. P. Singh, *Coord. Chem. Rev.*, 2020, **417**, 213369.

44 N. Fridman, M. Kaftory and S. Speiser, *Sens. Actuators, B*, 2007, **126**, 107–115.
45 T. Cai, A. Hatano, K. Kanatsu and T. Tomita, *J. Biochem.*, 2020, **167**, 463–471.
46 R. M. F. Batista, S. P. G. Costa, M. Belsley, C. Lodeiro and M. M. M. Raposo, *Tetrahedron*, 2008, **64**, 9230–9238.
47 R. M. F. Batista, S. P. G. Costa, M. Belsley and M. M. M. Raposo, *Dyes Pigm.*, 2009, **80**, 329–336.
48 J. Pina, J. S. Seixas De Melo, R. M. F. Batista, S. P. G. Costa and M. M. M. Raposo, *J. Phys. Chem. B*, 2010, **114**, 4964–4972.
49 R. C. M. Ferreira, S. P. G. Costa, H. Gonçalves, M. Belsley and M. M. M. Raposo, *New J. Chem.*, 2017, **41**, 12866–12878.
50 B. Pedras, R. M. F. Batista, L. Tormo, S. P. G. Costa, M. M. M. Raposo, G. Orellana, J. L. Capelo and C. Lodeiro, *Inorg. Chim. Acta*, 2012, **381**, 95–103.
51 X. Moreira, P. Santos, M. A. F. Faustino, M. M. M. Raposo, S. P. G. Costa, N. M. M. Moura, A. T. P. C. Gomes, A. Almeida and M. G. P. M. S. Neves, *Dyes Pigm.*, 2020, **178**, 108330.
52 E. Oliveira, R. M. F. Baptista, S. P. G. Costa, M. M. M. Raposo and C. Lodeiro, *Inorg. Chem.*, 2010, **49**, 10847–10857.
53 R. M. F. Batista, E. Oliveira, S. P. G. Costa, C. Lodeiro and M. M. M. Raposo, *Tetrahedron*, 2011, **67**, 7106–7113.
54 R. M. F. Batista, E. Oliveira, S. P. G. Costa, C. Lodeiro and M. M. M. Raposo, *Talanta*, 2011, **85**, 2470–2478.
55 C. Marín-Hernández, L. E. Santos-Figueroa, M. E. Moragues, M. M. M. Raposo, R. M. F. Batista, S. P. G. Costa, T. Pardo, R. Martínez-Máñez and F. Sancenón, *J. Org. Chem.*, 2014, **79**, 10752–10761.
56 C. I. C. Esteves, M. M. M. Raposo and S. P. G. Costa, *Dyes Pigm.*, 2016, **134**, 258–268.
57 C. I. C. Esteves, R. M. F. Batista, M. M. M. Raposo and S. P. G. Costa, *Dyes Pigm.*, 2016, **135**, 134–142.
58 H. E. Okda, S. El Sayed, R. C. M. Ferreira, S. P. G. Costa, M. M. Raposo, R. Martínez-Máñez and F. Sancenón, *Dyes Pigm.*, 2018, **159**, 45–48.
59 H. E. Okda, S. El Sayed, I. Otri, R. C. M. Ferreira, S. P. G. Costa, M. M. M. Raposo, R. Martínez-Máñez and F. Sancenón, *Dyes Pigm.*, 2019, **162**, 303–308.
60 H. E. Okda, S. El Sayed, R. C. M. Ferreira, R. C. R. Gonçalves, S. P. G. Costa, M. M. M. Raposo, R. Martínez-Máñez and F. Sancenón, *New J. Chem.*, 2019, **43**, 7393–7402.
61 H. E. Okda, S. El Sayed, I. Otri, R. C. M. Ferreira, S. P. G. Costa, M. M. M. Raposo, R. Martínez-Máñez and F. Sancenón, *Polyhedron*, 2019, **170**, 388–394.
62 Y. Ge, P. Wei, T. Wang, X. Cao, D. Zhang and F. Li, *Sens. Actuators, B*, 2018, **254**, 314–320.
63 A. J. Beneto, V. Thiagarajan and A. Siva, *RSC Adv.*, 2015, **5**, 67849–67852.
64 E. Horak, P. Kassal, M. Hranjec and I. M. Steinberg, *Sens. Actuators, B*, 2018, **258**, 415–423.
65 D. Pfeifer, I. Klimant and S. M. Borisov, *Chem. -Eur. J.*, 2018, **24**, 10711–10720.
66 R. P. C. L. Sousa, B. Ferreira, M. Azenha, S. P. G. Costa, C. J. R. Silva and R. B. Figueira, *Polymers*, 2020, **12**, 371.
67 B. R. Gomes, R. B. Figueira, S. P. G. Costa, M. M. M. Raposo and C. J. R. Silva, *Polymers*, 2020, **12**, 2671.
68 J. V. Morris, M. A. Mahaney and J. R. Huber, *J. Phys. Chem.*, 1976, **80**, 969–974.
69 D. Yanover and M. Kaftory, *Acta Crystallogr., Sect. E: Struct. Rep. Online*, 2009, **65**, o711.
70 F. Recio, C. Alonso, L. Gaillet and M. Sánchez Moreno, *Corros. Sci.*, 2011, **53**, 2853–2860.
71 M. Sánchez, M. C. Alonso, P. Cecílio, M. F. Montemor and C. Andrade, *Cem. Concr. Compos.*, 2006, **28**, 256–266.
72 J. Coates, in *Encyclopedia of Analytical Chemistry*, American Cancer Society, 2006.
73 S. D. F. C. Moreira, C. J. R. Silva, L. A. S. A. Prado, M. F. M. Costa, V. I. Boev, J. Martín-Sánchez and M. J. M. Gomes, *J. Polym. Sci., Part B: Polym. Phys.*, 2012, **50**, 492–499.
74 B. Arkles and G. Larson, *Silicon Compounds: Silanes & Silicones*, Gelest Inc., Morrisville PA, 3rd edn, 2013.
75 V. Bekiari, P. Lianos, U. Lavrencic Stangar, B. Orel and P. Judeinstein, *Chem. Mater.*, 2000, **12**, 3095–3099.
76 L. D. Carlos, V. de Zea Bermudez, R. A. Sá Ferreira, L. Marques and M. Assunção, *Chem. Mater.*, 1999, **11**, 581–588.
77 J. R. Macdonald, *Impedance Spectroscopy Emphasizing Solid Materials and Analysis*, John Wiley & Sons, Ltd, New York, NY, USA, 1987.
78 R. B. Figueira, C. J. Silva, E. V. Pereira and M. M. Salta, *J. Electrochem. Soc.*, 2013, **160**, C467–C479.
79 R. B. Figueira, C. J. Silva, E. V. Pereira and M. M. Salta, *J. Electrochem. Soc.*, 2014, **161**, C349–C362.
80 M. E. Orazem and B. Tribollet, *Electrochemical Impedance Spectroscopy*, Wiley, 2008.
81 B. Hirschorn, M. E. Orazem, B. Tribollet, V. Vivier, I. Frateur and M. Musiani, *Electrochim. Acta*, 2010, **55**, 6218–6227.
82 U. Thanganathan, *J. Mater. Chem.*, 2012, **22**, 9684–9689.
83 N. M. José, L. A. S. de Almeida Prado, M. A. Schiavon, S. U. A. Redondo and I. V. P. Yoshida, *J. Polym. Sci., Part B: Polym. Phys.*, 2007, **45**, 299–309.
84 L. A. S. A. De Prado, I. L. Torriani and I. V. P. Yoshida, *J. Polym. Sci., Part A: Polym. Chem.*, 2010, **48**, 1220–1229.
85 H. F. W. Taylor, C. Famy and K. L. Scrivener, *Cem. Concr. Res.*, 2001, **31**, 683–693.